

# Central Runge-Kutta Schemes for Conservation Laws

Lorenzo Pareschi<sup>†</sup> Gabriella Puppo<sup>‡</sup>  
Giovanni Russo<sup>§</sup>

## Abstract

In this work, a new formulation for central schemes based on staggered grids is proposed. It is based on a novel approach, in which first a time discretization is carried out, followed by the space discretization. The schemes obtained in this fashion have a simpler structure than previous central schemes. For high order schemes, this simplification results in higher computational efficiency. In this work, schemes of order 2 to 5 are proposed and tested, although CRK schemes of any order of accuracy can be constructed in principle. The application to systems of equations is carefully studied, comparing algorithms based on a componentwise extension of the scalar scheme, and algorithms based on projection along characteristic directions.

**Key words.** Hyperbolic systems, central difference schemes, high-order accuracy, WENO reconstruction, Runge-Kutta methods.

**AMS(MOS) subject classification.** 65M06, 35L60, 65L06, 76M12.

## 1 Introduction

Shock capturing schemes for the numerical approximation of systems of conservation laws have been an active field of research for the last thirty years (see for example the book by LeVeque [14] or the review articles by Tadmor [35], and Shu [30]).

Several classifications of the different schemes are possible. Here, we only consider shock capturing finite volume schemes: for these schemes, the conservation laws are integrated in space on cells of width  $h$ . Thus the equation is transformed in an evolution equation for the cell averages of the solution. In this formulation, to update the cell averages, it is necessary to evaluate numerical flux functions at the edge of each cell. This goal can be achieved by extracting information on point values from knowledge of the cell averages. This is the mission of reconstruction algorithms, whose task is precisely to compute the pointwise value of the solution as a function of position, at a given time, starting from the cell averages.

In this work we are interested in black-box schemes, i.e. schemes that can be implemented with very little knowledge of the structure of the system of conservation laws. In particular we mention those schemes based on the Local Lax Friedrichs flux, as reviewed in [30], central schemes, see [35] and relaxation schemes [9]. All these schemes enjoy the lack of need for Riemann solvers or complicated flux splittings.

From the pioneering works of Nessyahu and Tadmor in [20] and Sanders and Weiser [28] an extensive literature on central schemes has developed. These schemes are obtained by integrating the conservation law in space and time on control volumes which are staggered with respect to the cells on which the cell averages are based. In this fashion, the discontinuities in the pointwise solution produced by the reconstruction algorithm are located at the center of the staggered control volumes. As a consequence, the solution is smooth at the edges of the control volumes, thus enabling a simple construction of the numerical fluxes.

---

<sup>†</sup>Dipartimento di Matematica, Università di Ferrara, Via Machiavelli 35, 44100 Ferrara, Italy. [pareschi@dm.unife.it](mailto:pareschi@dm.unife.it)

<sup>‡</sup>Dipartimento di Matematica, Politecnico di Torino, Corso Duca degli Abruzzi 24, 10129 Torino, Italy. [puppo@calvino.polito.it](mailto:puppo@calvino.polito.it)

<sup>§</sup>Dipartimento di Matematica ed Informatica, Università di Catania, Viale Andrea Doria 6, 95125 Catania, Italy. [russo@dm.unict.it](mailto:russo@dm.unict.it)

Thanks to the appeal of the simplicity of this approach, the originally second order central staggered scheme has been extended to higher order schemes (up to order 8, as far as our knowledge goes), see [4], [15], [26], and to multidimensional computations on structured [1], [8], [17], and unstructured [2] grids. The success of central schemes based on staggered grids has prompted applications in several areas, such as semiconductor modeling [25], kinetic models [21], extended thermodynamics [19], [21], Hamilton-Jacobi equations [18]. See also [27] and references therein.

High order central schemes can be constructed by performing a reconstruction of the field from cell averages, and using this reconstruction for computing the staggered cell average, the pointwise value of the function from cell averages, and the space derivative of the flux function. High order reconstructions can be obtained using ENO [4] or WENO [15] technique applied to central schemes. The computation of the integral of the flux on the border of the cell is obtained by using a suitable quadrature formula, and the value of the field at the nodes of the quadrature formula are obtained by using a Runge-Kutta method with Natural Continuous Extension [37].

Although non staggered WENO finite volume and staggered central WENO schemes seem quite different, there are in fact some similarities between them. Both approaches, for example, do not require the solution of the (exact or approximate) Riemann problem (if a suitable numerical flux function, such as Local Lax-Friedrichs is used in the WENO scheme). In [10], a semidiscrete second order finite volume scheme is derived, starting from a discrete central scheme. This derivation shows the similarity of the two approaches.

Another common feature is that both approaches would benefit from the use of characteristic variables in the reconstruction. An interesting comparison between them is performed in [26].

In this work, we present a new family of high order central schemes, based on staggered grids. The new Central Runge Kutta (or CRK) schemes are obtained starting from the equation for the evolution of cell averages on staggered cells. This is discretized in time by a special and novel use of Runge-Kutta methods, in which the stage values are computed pointwise at the edge of the cell, and the final value for the staggered cell average is computed by a conservative scheme. The result is a new formulation which simplifies the structure of traditional central schemes based on staggered grids. Some known central schemes, such as the Nessyahu Tadmor scheme, can be written in the CRK formulation. For schemes of order higher than 3, however, CRK schemes are more efficient than older central schemes, because they require a smaller number of function evaluations per time step. This improvement is due to the fact that in the CRK formulation it is not necessary to use a quadrature rule in time for the fluxes, which in turn implied the evaluation of Natural Continuous Extension.

We construct second and third order CRK schemes. Moreover, using a piecewise parabolic WENO reconstruction we provide fourth and even fifth order schemes (negative weights are properly treated, as in [29]). In principle, schemes of any order of accuracy can be constructed.

This paper is organized as follows. §2 opens with a review of the main structure of central schemes. This section also contains the construction of CRK schemes. The section ends with a study of the linear stability properties of CRK schemes.

We present numerical results for the scalar case in §3. Here we show accuracy results for 1D and 2D test problems; a 2D test with shock interactions is also shown to illustrate the non oscillatory properties of CRK schemes.

We describe the implementation of CRK schemes in the case of systems of equations in §4. We show results on a few typical test problems, in 1D and 2D tests. Finally, we compare the behavior of componentwise application of the scalar scheme versus a more accurate (but costly) implementation of the scheme along the direction of characteristic variables. The idea of applying characteristic projection to central schemes [26] is quite effective in some applications, but it is quite foreign to the central schemes philosophy, because it damages the black box structure of these schemes. However, it is interesting to see that, once more information on the structure of the system of equations is available, the numerical solution provided by central schemes can be improved, especially near discontinuities of the solution, making these schemes competitive with flux splitting schemes, which are more tailored to the particular system under consideration. Moreover, the additional cost of the computation along characteristic variables can be drastically reduced, provided an adaptive strategy is considered, as in [24].

## 2 Description of CRK schemes

We consider the system of equations

$$u_t + f_x(u) = 0, \quad (2.1)$$

with  $u \in R^m$ ,  $f : R^m \rightarrow R^m$  continuously differentiable. We suppose that the Jacobian of  $f$ ,  $A(u) = f'(u)$  has real eigenvalues and a complete set of eigenvectors.

Let  $\Delta t$  and  $h$  be the mesh widths in time and space, with  $\lambda = \Delta t/h$ . Let  $I_j = [x_j - \frac{h}{2}, x_j + \frac{h}{2}]$  be the interval of width  $h$  centered around the grid point  $x_j$ .

Introduce the cell average of  $u$  over the interval  $I_j = [x_j - \frac{h}{2}, x_j + \frac{h}{2}]$  at time  $t^n$ :

$$\bar{u}_j^n = \frac{1}{h} \int_{x_j - h/2}^{x_j + h/2} u(x, t^n) dx. \quad (2.2)$$

Integrating the conservation law (2.1) on  $I_j$  and dividing by  $h$ , one finds:

$$\left. \frac{d\bar{u}}{dt} \right|_j = -\frac{1}{h} [f(u(x_{j+1/2}, t)) - f(u(x_{j-1/2}, t))]. \quad (2.3)$$

This equation is exact and it gives the evolution in time of the cell averages. Finite volume schemes are based on the discretization of (2.3). These schemes approximate the flux appearing in (2.3) by a numerical flux function which depends on the cell averages. The final system of ordinary differential equations for  $\bar{u}(t)$  is then discretized in time, providing the cell averages  $\{\bar{u}^{n+1}\}$ , at time  $t^{n+1}$ , starting from the old cell averages  $\{\bar{u}^n\}$  at time  $t^n$ .

A key point in both upwind and central schemes is the reconstruction step. From the cell averages  $\{\bar{u}^n\}$ , it is necessary to reconstruct the initial data  $u^n(x)$ . This information is needed to evaluate the right hand side of (2.3). Typically, starting from  $\{\bar{u}^n\}$ , one computes a piecewise polynomial function of the form:

$$u^n(x) = R(x; \{\bar{u}^n\}) = \sum_j P_j^d(x) \chi_{I_j}(x). \quad (2.4)$$

where  $P_j^d(x)$  is a polynomial of degree  $d$ , and  $\chi_{I_j}$  is the characteristic function of interval  $I_j$ .

For the scheme to be conservative, it is necessary that  $u^n(x)$  interpolates the data  $\{\bar{u}^n\}$  in the sense of cell averages. The reconstruction in general will be discontinuous at the end points of the interval  $I_j$ . In general, to increase the accuracy of the scheme, it is necessary to increase the degree of the interpolating polynomial. However, with WENO approach [7], it is possible to obtain high order accurate schemes with relatively low degree interpolating polynomials. The main difficulty in the design of reconstruction algorithms is that the reconstructed function  $u^n(x)$  must be non-oscillatory, in order to prevent the onset of spurious oscillations. A survey of several reconstruction algorithms can be found in [30].

In central schemes based on staggered grids, the conservation law is integrated on the staggered control volume:  $V_{j+1/2}^n = [x_j, x_{j+1}] \times [t^n, t^n + \Delta t]$ . Integrating (2.1) in space and time on  $V_{j+1/2}^n$  and dividing by  $h$ , one finds:

$$\bar{u}_{j+1/2}^{n+1} = \bar{u}_{j+1/2}^n - \frac{1}{h} \int_0^{\Delta t} [f(u(x_{j+1}, t^n + \tau)) - f(u(x_j, t^n + \tau))]. \quad (2.5)$$

The first term on the RHS  $\bar{u}_{j+1/2}^n$  is approximated by integrating the reconstruction exactly on  $[x_j, x_{j+1}]$ :

$$\bar{u}_{j+1/2}^n = \frac{1}{h} \int_{x_j}^{x_{j+1}} u^n(x) dx = \frac{1}{h} \int_{x_j}^{x_{j+1/2}} P_j^d(x) dx + \frac{1}{h} \int_{x_{j+1/2}}^{x_{j+1}} P_{j+1}^d(x) dx. \quad (2.6)$$

Since  $u$  is smooth at  $x_j$  and  $x_{j+1}$ , if the time step is small enough, the integral in time of the fluxes can be accurately evaluated through quadrature. The values of  $u$  at the nodes of the quadrature formula are predicted integrating the system of ODE's

$$\left. \frac{du}{dt} \right|_{x_j} = -f_x(u)|_{x_j},$$

using again the smoothness of  $u$  at  $x_j$ .

An example is the second order Nessyahu-Tadmor scheme, which is characterized by a piecewise linear reconstruction, while the fluxes are integrated with the midpoint rule, and the value of  $u$  at the midpoint is predicted with Taylor expansion. For a thorough review on high order central schemes, see [27].

Before describing Central Runge Kutta schemes, we need to set a suitable notation for Runge-Kutta schemes applied to initial value problems. Therefore let:

$$\begin{cases} y' &= g(y), \\ y(t_0) &= y_0. \end{cases}$$

Apply to the initial value problem above an explicit Runge-Kutta scheme with  $\nu$  stages:

$$y^{n+1} = y^n + \Delta t \sum_{i=1}^{\nu} b_i K^{(i)}.$$

The  $K^{(i)}$  are called *Runge-Kutta fluxes* and are defined by:

$$K^{(i)} = g(y^{(i-1)}) \quad \text{with} \quad y^{(0)} = y^n, \quad i = 1, \dots, \nu$$

where the  $y^{(i)}$  will be called *intermediate values*, and, for an explicit scheme, are given by:

$$y^{(i)} = y^n + \Delta t \sum_{l=1}^i a_{i,l} K^{(l)}, \quad i = 1, \dots, \nu - 1.$$

The matrix  $A = (a_{i,l})$ , and the vector  $b$  define uniquely the RK scheme. With the present notation,  $A$  is a  $\nu - 1 \times \nu - 1$  lower triangular matrix, with non zero elements on the diagonal. Note that this notation is slightly different than the usual one adopted for describing Runge-Kutta schemes.

We are now ready to describe our new CRK schemes.

In Central Runge Kutta schemes, the conservation law is integrated on the interval  $I_{j+1/2} = [x_j, x_{j+1}]$ . We obtain the exact equation:

$$\left. \frac{d\bar{u}}{dt} \right|_{j+1/2} = -\frac{1}{h} [f(u(x_{j+1}, t)) - f(u(x_j, t))]. \quad (2.7)$$

Note the parallel with equation (2.3). Next, this equation is discretized in time with a Runge-Kutta scheme. Thus the updated solution will be given by:

$$\bar{u}_{j+1/2}^{n+1} = \bar{u}_{j+1/2}^n - \lambda \sum_{i=1}^{\nu} b_i K_{j+1/2}^{(i)}, \quad (2.8)$$

with:

$$K_{j+1/2}^{(i)} = f(u_{j+1}^{(i-1)}) - f(u_j^{(i-1)}) \quad \text{with} \quad u_j^{(0)} = u^n(x_j). \quad (2.9)$$

To evaluate the intermediate states,  $u_j^{(i)}$ , we exploit the fact that the reconstruction  $u^n(x)$  is smooth except for jumps at the cell edges,  $x_{j\pm 1/2}$ . Thus,  $u(x_j, t)$  remains smooth for  $t \in [t^n, t^n + \Delta t]$ , if  $\Delta t$  is small enough. As in all central schemes based on staggered grids, we can therefore evaluate the intermediate states  $u_j^{(i)}$  integrating the conservation law (2.1) in its differential form, namely:  $u_t = -f_x(u)$ . Thus:

$$u_j^{(i)} = u_j^{(0)} + \Delta t \sum_{l=1}^i a_{i,l} \hat{K}_j^{(l)}, \quad i = 1, \dots, \nu - 1, \quad (2.10)$$

with the Runge-Kutta fluxes:

$$\hat{K}_j^{(l)} = -\left. \frac{\partial f(u^{(l-1)})}{\partial x} \right|_j \quad \text{and} \quad u_j^{(0)} = u^n(x_j) \quad l = 1, \dots, \nu - 1. \quad (2.11)$$

At this stage, we have completed the time discretization of the scheme. Note that the above scheme can clearly be written in conservation form.

We now need to specify the space discretization, which is obtained with reconstruction techniques. The reconstruction must yield the following quantities:

- Starting from the cell averages  $\{\bar{u}_j^n\}$ , compute the staggered cell averages,  $\{\bar{u}_{j+1/2}^n\}$ , appearing in (2.8), as defined in (2.6).
- Starting from the cell averages  $\{\bar{u}_j^n\}$ , compute the point values,  $\{u_j^n = u^n(x_j)\}$ , which are needed to compute the start-up values  $u_j^{(0)}$  in (2.10).
- Starting from the intermediate values  $\{u_j^{(i)}\}$ , compute the derivative of the fluxes  $\{f_x(u^{(i)})|_j\}$ . These quantities form the Runge-Kutta fluxes in (2.11).

Note that we can use different interpolation algorithms for each quantity we need to reconstruct. According to our numerical evidence (see also [26]) the key step is the reconstruction of  $\{\bar{u}_{j+1/2}^n\}$ .

The algorithm for CRK schemes can be conveniently written as a three step method, as follows:

1. **Reconstruction step:** From the cell averages  $\{\bar{u}_j^n\}$ , compute the reconstruction  $u^n(x)$ . Use this to evaluate  $u_j^{(0)} = u^n(x_j)$  and  $\bar{u}_{j+1/2}^n$ .
2. **Predictor step:** Compute the intermediate states  $u_j^{(i)}$ :  
For  $i = 1, \dots, \nu - 1$ :
  - Compute  $f(u_j^{(i-1)}) \forall j$ ;
  - Apply a suitable non-oscillatory interpolation to yield  $\hat{K}_j^{(i)} = -f_x(u^{(i-1)})_j$ ;
  - Compute  $u_j^{(i)} = u_j^{(0)} + \Delta t \sum_{l=1}^i a_{i,l} \hat{K}_j^{(l)}$ .
3. **Corrector step:** Assemble the fluxes  $K_{j+1/2}^{(i)}$  defined above, and update the cell averages on the staggered grid:

$$\bar{u}_{j+1/2}^{n+1} = \bar{u}_{j+1/2}^n - \lambda \sum_{i=1}^{\nu} b_i K_{j+1/2}^{(i)},$$

Note that the computation of  $\hat{K}_j^{\nu}$  is not required. This improves the efficiency of the scheme, because it requires one less interpolation per time step, with respect to previous high order Central WENO schemes. We end this section giving all details needed to code the CRK schemes we will test in the next sections.

## 2.1 A second order scheme: CRK2

The second order scheme we propose has Nessyahu-Tadmor piecewise linear reconstruction:

$$u^n(x) = \sum_j (\bar{u}_j^n + u'_j(x - x_j)) \chi_{I_j}(x),$$

where  $u'_j$  is an approximate slope, computed for instance with the MinMod limiter. Time integration is given by Heun's scheme. Therefore the scheme is:

$$\begin{aligned} \bar{u}_{j+1/2}^n &= \frac{1}{2}(\bar{u}_j^n + \bar{u}_{j+1}^n) + \frac{1}{8}(u'_j - u'_{j+1}) \\ u_j^{(1)} &= \bar{u}_j^n - \Delta t f_x(\bar{u}_j^n) \\ \bar{u}_{j+1/2}^{n+1} &= \bar{u}_{j+1/2}^n - \frac{\lambda}{2}(f(\bar{u}_{j+1}^n) + f(u_{j+1}^{(1)}) - f(\bar{u}_j^n) - f(u_j^{(1)})), \end{aligned}$$

where, for instance,

$$f_x(\bar{u}_j^n) = \frac{1}{h} \text{MinMod}(f(\bar{u}_{j+1}^n) - f(\bar{u}_j^n), f(\bar{u}_j^n) - f(\bar{u}_{j-1}^n)).$$

It is easy to prove that this scheme coincides with the Nessyahu Tadmor scheme in the case of linear advection. Moreover, following the same steps appearing in [20], it is easy to prove that the CRK2 scheme is TVD, under a stricter CFL condition, provided that suitable limiters are used to compute both  $\bar{u}_j^n$  and  $f_x(u)|_j$ . Note that if the Modified Euler rule is used for time integration instead of the TVD Heun scheme, the CRK2 scheme coincides with Nessyahu-Tadmor scheme.

## 2.2 Higher order schemes: CRK3, CRK4, CRK5

In this section, we describe a third, fourth and fifth order scheme (respectively: CRK3, CRK4, and CRK5). All these schemes are built with Central WENO reconstructions.

We start describing how  $\bar{u}_{j+1/2}^n$  is computed. Then we will sketch how point values and flux derivatives are constructed.

In all three cases, the reconstruction from cell averages is a non linear convex combination of three interpolating polynomials. On the interval  $I_j$ :

$$u^n(x)|_{I_j} = R_j(x) = w_j^{-1}P_{j-1}(x) + w_j^0P_j(x) + w_j^{+1}P_{j+1}(x), \quad (2.12)$$

where the  $w_j^k$  are the non linear weights, which satisfy  $\sum_k w_j^k = 1$ .

For the third order scheme, [16],  $P_{j-1}$  and  $P_{j+1}$  are two linear functions, while  $P_j$  is a parabola. For the 4th and 5th order schemes, all polynomials  $P_{j+k}(x)$ ,  $k = -1, 0, +1$  are parabolas. In all schemes considered therefore the reconstruction  $u^n(x)$  is piecewise parabolic. The reconstruction is conservative, in the sense that:

$$\frac{1}{h} \int_{x_{j+k-1/2}}^{x_{j+k+1/2}} R_j(x) dx = \bar{u}_{j+k} \quad k = -1, 0, +1.$$

The weights  $w_j^k$  are determined in order to:

- maximize accuracy in smooth regions
- prevent the onset of spurious oscillations.

Following [7], we define the weights with the following formulas:

$$w_j^k = \frac{\alpha_j^k}{\sum_{l=-1}^1 \alpha_j^l} \quad \text{where} \quad \alpha_j^k = \frac{C^k}{(\epsilon + \text{IS}_j^k)^2}. \quad (2.13)$$

The  $C^k$ 's are called accuracy constants. They are determined in order to maximize accuracy in smooth regions, and they depend on the particular quantity being reconstructed, see Table 2.1.

The parameter  $\epsilon$  prevents a vanishing denominator. It is  $\epsilon = 10^{-4}$  for the third order scheme, while  $\epsilon = 10^{-6}$  for the 4-th and 5-th order schemes.

Finally,  $\text{IS}_j^k$ ,  $k = -1, 0, 1$  are called smoothness indicators.  $\text{IS}_j^k$  is a measure of the regularity of the polynomial  $P_{j+k}$  on the interval  $I_j$ . It is defined (see [7]), as a rescaled measure of the  $H^2$  seminorm of the polynomial on  $I_j$ :

$$\text{IS}_j^k = \sum_{l=1}^2 \int_{x_{j-1/2}}^{x_{j+1/2}} h^{2l-1} \left( \frac{d^l P_{k+j}}{dx^l} \right)^2 dx, \quad k = -1, 0, 1. \quad (2.14)$$

Thus  $\text{IS}_j^k = O(h^2)$  on smooth regions, while  $\text{IS}_j^k = O(1)$  if the data in the stencil of  $P_{k+j}$  contain a jump discontinuity. As a consequence of the normalization factor,  $w_j^k = C^k + O(h^s)$ , if the stencil  $S_{j+k}$

Scheme	$C^{-1}$	$C^0$	$C^{+1}$	Accuracy
<i>Reconstruction of <math>\bar{u}_{j+1/2}^n</math></i>				
CRK3	1/4	1/2	1/4	$h^3$
CRK4	3/16	5/8	3/16	$h^5$
CRK5	3/16	5/8	3/16	$h^5$
<i>Reconstruction of <math>u^n(x_j)</math></i>				
CRK3	1/4	1/2	1/4	$h^3$
CRK4	3/16	5/8	3/16	$h^4$
CRK5	-9/80	49/40	-9/80	$h^5$
<i>Reconstruction of <math>f_x(u(x, \cdot)) _{x_j}</math></i>				
CRK3	1/4	1/2	1/4	$h^2$
CRK4	1/6	2/3	1/6	$h^4$
CRK5	1/6	2/3	1/6	$h^4$

Table 2.1: Accuracy constants

*Coefficients of Runge-Kutta schemes*

Scheme	A	b
RK2	1	1/2 1/2
RK3	1 1/4 1/4	1/6 1/6 2/3
RK4	1/2 0 1/2 0 0 1	1/6 1/3 1/3 1/6
RK5	1/2 3/16 1/16 0 0 1/2 0 -3/16 6/16 9/16 1/7 4/7 6/7 -12/7 8/7	7/90 0 32/90 12/90 32/90 7/90

Table 2.2: Coefficients of Runge-Kutta schemes

on which  $P_{j+k}$  is defined contains smooth data ( $s = 1$  for the third order reconstruction, while  $s = 2$  in the 4-th and 5-th order reconstructions).

Particular care is needed in the reconstruction of point values for the new fifth order CRK5 scheme. In this case in fact two accuracy constants for the reconstruction of point values are negative (see Table 2.1), and a straightforward application of the algorithm with the non linear weights yields a scheme that can become unstable, especially in the presence of interactions between discontinuities. For more details, see [16], for the third order scheme, [15] for the fourth order scheme, and [27] for the splitting of the weights for the 5th order method.

The time integration is carried out with the Runge-Kutta schemes listed in Table 2.2. RK3 is the third order TVD Runge-Kutta scheme appearing in [32]. RK4 is the standard 4-th order Runge-Kutta scheme, while the 5-th order scheme can be found in [11].

**Remark:** CRK2 and CRK3 have the same operation count as the Nessyahu-Tadmor and the Compact Central WENO schemes, respectively. It is also easy to prove that they actually coincide with the previously derived schemes, in the case of the linear advection equation.

CRK4 instead is more efficient than the previous Central WENO scheme, [15] from which it inherits its reconstruction algorithms. In fact CRK4 requires one interpolation step less than the C-WENO scheme for each time step. However, the numerical results are almost indistinguishable from those obtained with the older scheme.

A fifth order central scheme such as CRK5 had not previously appeared.

### 2.3 Linear stability analysis

The CFL condition for all central staggered schemes is:

$$\lambda \leq \lambda_0 \frac{1}{\max(|f'(u)|)} \leq \frac{1}{2} \frac{1}{\max(|f'(u)|)}.$$

In fact in this case, the waves issuing from the interaction of the jumps in the reconstruction at  $x_{j+1/2}$  do not have the time to reach the edges of the staggered control volumes  $V_{j+1/2} = [x_j, x_{j+1}] \times [t^n, t^{n+1}]$  on which the conservation law is integrated. Thus it is possible to assume that the solution remains smooth along the segments  $x_j \times [t^n, t^n + \Delta t]$ , if  $\Delta t \leq \lambda h$ .

In this section, we compute the linear stability constraints on  $\lambda_0$  obtained with von Neumann stability analysis. In any case, we will have  $\lambda_0 \leq 1/2$ .

To apply Von Neumann analysis, we consider the *linear* schemes we obtain if all reconstructions are computed as:

$$R_j(x) = \sum_{k=-1}^1 C^k P_{j+k}(x),$$

where the constants  $C^k$  are given in Table 2.1 and the polynomials  $P_{j+k}$  were constructed in the previous subsection.

We compute the amplification factor  $\rho(\xi)$  of a data of the form  $\bar{u}_j = \exp(ijh\xi)$  after one time step.

Note that the computation is quite straightforward for CRK schemes (although long and tedious), thanks to the simplicity of the structure of these schemes. In fact we no longer need to deal with quadrature rules in time for the fluxes and Natural Continuous Extensions, as in previous Central schemes. This fact makes the analysis of these schemes much simpler than before.

We list below the Courant numbers  $\lambda_0$  we have found for each scheme. For  $\lambda \leq \lambda_0$ ,  $\rho(\xi) \leq 1$  for all wave numbers  $\xi$ :

$$\begin{aligned} \text{CRK2} : \quad \lambda_0 &= \frac{1}{2} = 0.5 \\ \text{CRK3} : \quad \lambda_0 &= \frac{3}{7} \simeq 0.42 \\ \text{CRK4} : \quad \lambda_0 &= \frac{12}{25} = 0.48 \\ \text{CRK5} : \quad \lambda_0 &= \frac{60}{149} \simeq 0.40. \end{aligned} \tag{2.15}$$

Note that in all cases, linear stability gives a result very close to the actual CFL limit of these schemes, i.e. 0.5.

We have also implemented the Runge-Kutta schemes proposed in [33] and designed to optimize stability, but we have not found any improvement, in our case. This is probably due to the fact that the schemes in [33] were constructed for standard semidiscrete schemes.

## 3 Numerical results in the scalar case

In this section, we will show accuracy results on two classical test problems. We also discuss the extension of CRK schemes to 2D problems.

We have found experimentally that it is enough to compute the Smoothness Indicators only once per time step, during the reconstruction from cell averages. Therefore the non linear weights of the different reconstructions differ because each uses the proper accuracy constants, and the correct interpolation conditions, to compute the interpolation polynomials  $P_{j+k}$  entering the reconstruction. The Smoothness Indicators instead remain constant throughout the time step.

### 3.1 Accuracy results

Our first test problem is the linear advection equation  $u_t + u_x = 0$ , with initial condition:

$$u(x, t = 0) = \sin^4(\pi x),$$

*L<sup>1</sup> norm of the error and L<sup>1</sup> accuracy for CRK schemes*

<b>Error</b>	CRK2	CRK3	CRK4	CRK5
$N = 20$	0.1108	0.2280	0.7732E-01	0.15519
$N = 40$	0.3751E-01	0.6755E-01	0.9493E-02	0.2905E-01
$N = 80$	0.1430E-01	0.1197E-01	0.6664E-03	0.1498E-02
$N = 160$	0.4129E-02	0.8713E-03	0.3143E-04	0.3550E-04
$N = 320$	0.1129E-02	0.6951E-04	0.1958E-05	0.8617E-06
$N = 640$	0.2955E-03	0.7775E-05	0.1223E-06	0.2196E-07
<b>Order</b>				
$N = 20$	1.5634	1.7551	3.0258	2.4171
$N = 40$	1.3905	2.4960	3.8323	4.2776
$N = 80$	1.7928	3.7808	4.4059	5.3987
$N = 160$	1.8703	3.6477	4.0050	5.3647
$N = 320$	1.9344	3.1603	4.0007	5.2943

Table 3.1: Accuracy results in the  $L^1$  norm for the linear advection equation,  $T = 2$

on  $[-1, 1]$  with periodic boundary conditions. The computation is stopped at  $T = 2$ .

This test is interesting, because it can detect degradation of accuracy in some cases, see [31]. We show the results in Table 3.1 for the  $L^1$  norm.

Here,  $N$  is the number of grid points. In most cases, the mesh parameter was chosen as  $\lambda = 0.9\lambda_0$ , with  $\lambda_0$  given by the results of the linear stability analysis, (2.15), except for CRK5, which has  $\lambda = 0.8\lambda_0$ . For values of  $\lambda$  closer to  $\lambda_0$ , CRK5 yields large errors on coarse grids, while the errors are comparable to those shown in the present tables for finer grids. In this fashion, the accuracy is overestimated for values of  $\lambda$  larger than  $0.8\lambda_0$ .

The results for the  $L^\infty$  norm are very similar, except for the CRK2 scheme, where the clipping phenomenon of the MinMod limiter deteriorates accuracy to slightly more than first order. This of course is a familiar phenomenon for schemes based on slope limiters, when the exact solution exhibits local extrema. This problem with CRK2 could be avoided by using a more sophisticated slope limiter, such as the UNO limiter by Harten [5] as shown, for example, in [20], thus recovering full second order accuracy.

We note that all schemes studied have full accuracy in the  $L^1$  norm. The higher order CRK schemes do not degenerate to first order on local extrema and maintain full accuracy also in the  $L^\infty$  norm.

Analogous convergence rates are observed also for Burgers' equation, before shock formation.

Note that, as the grid is refined, high order schemes yield smaller errors than lower order schemes for a given value of  $N$ . High order schemes become effective, apparently, only on fine grids. CRK4 however is an exception: its errors are smaller than those obtained with lower order schemes on all grids considered.

### 3.2 Two dimensional extension

CRK schemes can be very easily extended to two and three dimensions. In this section we describe very briefly how two dimensional schemes can be obtained. As a case study, we will consider only the extension of the fourth order CRK4 scheme.

In principle, central schemes based on staggered grids can be applied to two dimensional triangular, unstructured grids, see for instance [2], where the second order Nessyahu-Tadmor scheme is extended to unstructured two-dimensional grids. The same holds for WENO reconstruction procedure, see [6]. In this work we will consider an extension based on uniform rectangular grids. In this case, the reconstruction is obtained simply through the tensor product of two one-dimensional reconstructions. The accuracy constants change, and can be found in [17], where the fourth order Central WENO reconstruction is described in detail. Time discretization is of course the same of the one-dimensional case.

*Error and accuracy for the 2D CRK4 scheme*

<b>N</b>	$L^1$ error	$L^1$ order	$L^\infty$ error	$L^\infty$ order
10	0.19828E-01	-	0.33884E-01	-
20	0.10382E-02	4.25	0.18823E-02	4.17
40	0.38051E-04	4.77	0.90756E-04	4.37
80	0.13179E-05	4.85	0.47165E-05	4.27
160	0.42994E-07	4.94	0.26761E-06	4.14

Table 3.2: Accuracy results for the 2D CRK4 scheme on the linear advection equation,  $T = 1$

First, we show a convergence test on a two-dimensional linear advection problem. Here the equation solved is:

$$u_t + u_x + u_y = 0 \quad u_0(x, y) = \sin^2(\pi x)\sin^2(\pi y) \quad (x, y) \in [0, 1]^2,$$

with periodic boundary conditions. The results appear in Table 3.2 and they show that CRK4 is clearly fourth order accurate in the  $L^1$  and the  $L^\infty$  norms.

Next, we consider the classical test in [1, 8], see Fig. 3.1.

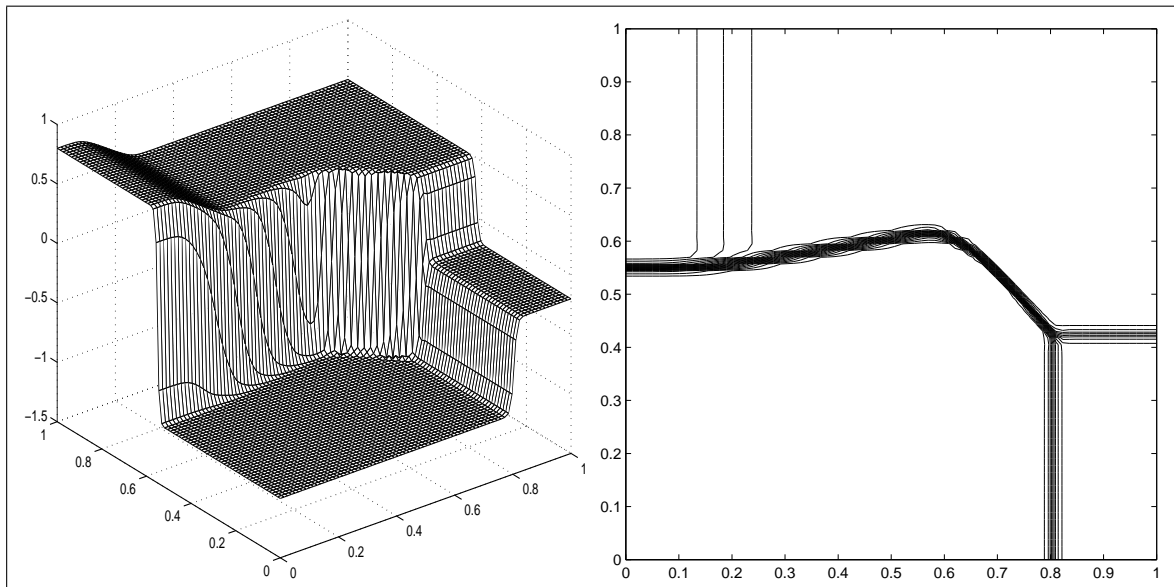


Figure 3.1: Burgers' equation.  $N = 80$ ,  $T = 0.5$ .

This test is based on the 2D Burgers' equation, on a truly 2D Riemann problem which yields three interacting shocks, and a rarefaction wave. Fig. 3.1 shows the solution obtained with an 80 by 80 grid at  $T = 0.5$ , with  $\lambda = 0.5$ . On the right, a contour plot, obtained with 20 level lines is shown. It is apparent that all shocks are resolved with sharp, oscillation-free transitions.

## 4 Systems of equations

In this section, we study the application of CRK schemes to systems of conservation laws. We start with results obtained with the componentwise application of CRK schemes. This procedure is fast, and it permits to apply the schemes easily to different systems of equations. In this case in fact, only the flux function and an estimate of the characteristic speeds must be provided. The tests show that the numerical solution converges, as the grid is refined, but spurious oscillations may arise, although their amplitude decreases under grid refinement.

Recently, Qiu and Shu [26] have shown with numerical evidence that the numerical solution improves if projection along characteristic directions is used at the beginning of each time step. The algorithm is quite costly, and part of the simplicity of central schemes is lost, because with this approach it is necessary to provide the flux function, and the matrix of right eigenvectors for the Jacobian of the flux, together with its inverse. However the improvements are indeed striking. We apply this idea to CRK schemes at the end of this section. A more efficient approach is described in [24].

The tests we will show are classical tests from gas dynamics. We review the notation used. The one-dimensional Euler's equations for an ideal gas consist of three conservation laws. The vector of unknowns is  $u = (\rho, \rho v, E)^T$ , where  $\rho$  is the density,  $v$  is the velocity and  $E$  is the total energy per unit volume, given by  $E = \frac{1}{2}\rho v^2 + \rho e$ , with  $e$  the internal energy, linked to the pressure  $p$  by the equation of state  $p = p(\rho, e)$ . For a polytropic gas  $p = \rho e(\gamma - 1)$ , with  $\gamma = c_p/c_v$ . The value  $\gamma = 7/5$ , valid for a biatomic gas such as air, has been used in the numerical tests. The flux is  $f(u) = (\rho v, \rho v^2 + p, v(E + p))$ .

#### 4.1 Componentwise application

The simplest approach to the integration of systems of conservation laws with CRK schemes is to apply the schemes component by component to each equation of system (2.1). It was found in [15] that the scheme gained in robustness if the Smoothness Indicators were the same for all components. For this reason a Global Smoothness Indicator was proposed, namely:

$$IS_k^j = \frac{1}{m} \sum_{r=1}^m \frac{1}{\|\bar{u}_r\|_2^2} \left( \sum_{l=1}^2 \int_{I_j} h^{2l-1} \left( \frac{d^l P_{j+k,r}}{dx^l} \right)^2 dx \right) \quad (4.1)$$

for  $k = -1, 0, 1$ . Here  $r$  denotes the  $r$ -th component of the solution and of the vector-valued interpolating polynomial. Comparing with (2.14), we see that the Global Smoothness Indicator is just a weighted average of the Smoothness Indicators given by each component. The weights in the average are chosen in order to obtain a dimensionless quantity. This ensures that the indicators are invariant with respect to changes in units of measure.

The first test we show is by Shu and Osher, [32]. It describes the interaction of an acoustic wave with a shock. The solution has a rich structure, which is better resolved by a high accuracy scheme. The initial condition is  $u = u_L$  for  $x \leq 0.1$ , and  $u = u_R$  for  $x > 0.1$ . The computational domain is  $[0, 1]$ , with free-flow boundary conditions. The left (L) and right (R) states are given by:

$$\begin{pmatrix} \rho \\ v \\ p \end{pmatrix}_L = \begin{pmatrix} 3.857143 \\ 2.629369 \\ 10.3333 \end{pmatrix} \quad \begin{pmatrix} \rho \\ v \\ p \end{pmatrix}_R = \begin{pmatrix} 1 + 0.2 \sin(50x) \\ 0 \\ 1 \end{pmatrix}$$

The reciprocal of the maximum characteristic speed for this flow is  $c \simeq 0.219$ . Thus we used the mesh ratio  $\lambda = 0.2\lambda_0$ , where the appropriate value of  $\lambda_0$  can be found, as usual, in (2.15). The solution is printed at  $T = 0.18$ . The results are shown in Fig. 4.1. The solid line is the reference solution, obtained with CRK4 and 1600 grid points. The dotted line is the numerical solution, computed using 400 grid points.

The figure shows clearly that there is a noticeable increase in resolution, using high order schemes. Although the difference between the numerical solutions obtained with CRK2 and CRK3 is very small, there is a very strong improvement with the 4th order scheme. In fact, the structure behind the strong shock is not resolved by the low order schemes. In contrast, its complexity is well represented by the 4th and the 5th order schemes, without need to use a very large number of grid points.

This test well illustrates the benefits of high order schemes, and it also points to their natural field of applications, namely simulations of possibly singular complex phenomena.

This figure also illustrates a fact that appears in all tests we have performed. The best schemes in the CRK class we are considering are CRK2 and CRK4. While there is a strong improvement passing from the second order CRK2 scheme to the fourth order CRK4 scheme, there is almost no improvement passing from second to third order, or from fourth to fifth order.

There are several reasons to explain this result. On one hand, CRK2 and CRK4 enjoy the highest CFL numbers, see (2.15). This gives a smaller numerical viscosity. The reconstruction of CRK3 is

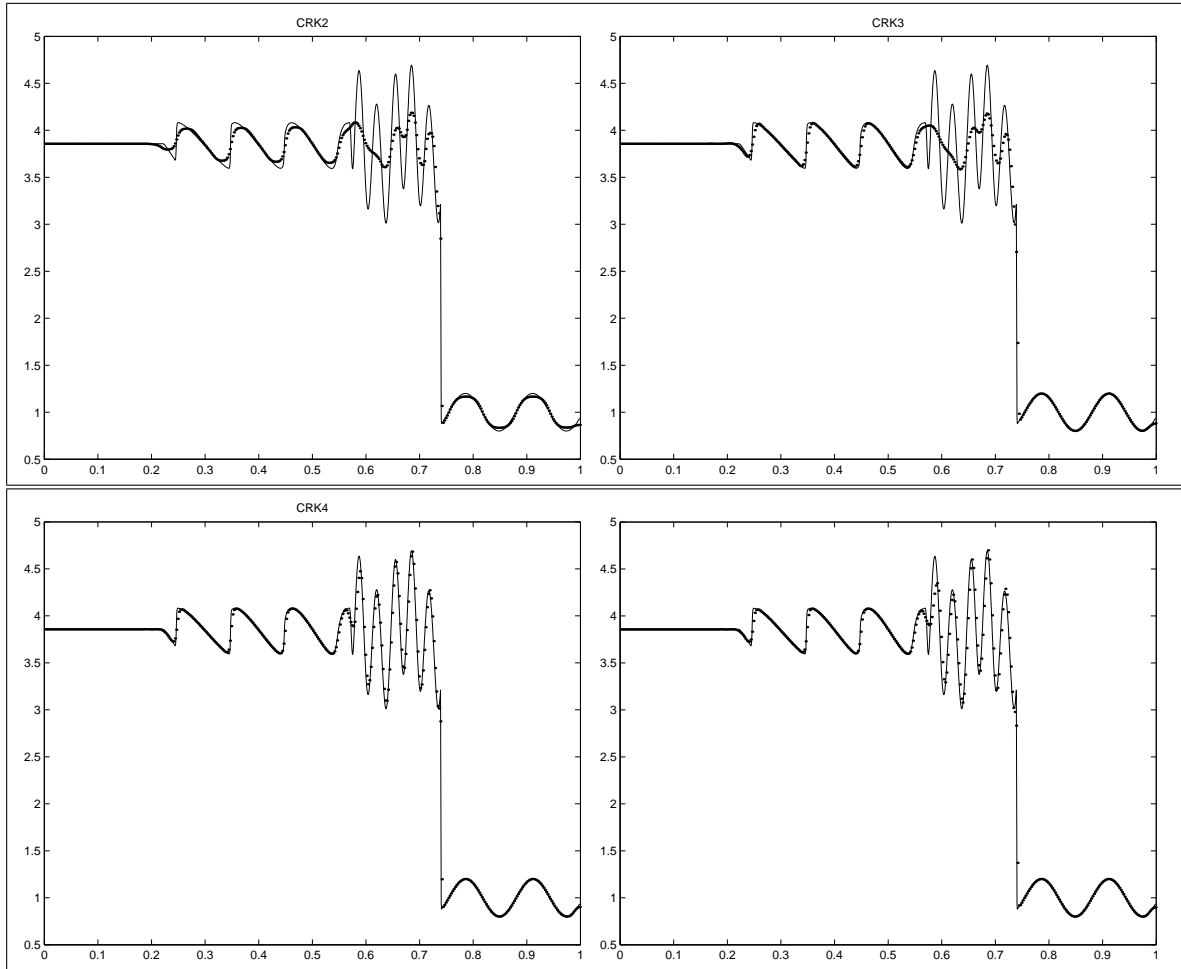


Figure 4.1: Shock-acoustic interaction  $\lambda = 0.2\lambda_0$ . Solution given by CRK2, CRK3, CRK4, and CRK5 for  $N = 400$ .

composed of two linear and a quadratic polynomial; when the weights are not optimal, the two linear functions are not balanced by the central parabola, and the reconstruction deteriorates to second order, thus giving results which are close to CRK2. CRK3 improves dramatically if non linear weights are used only close to discontinuities, see [23]: in this case in fact the optimal weights are used in regions of smooth flow, enhancing accuracy.

For CRK4, we note that the reconstruction of the staggered cell averages is actually fifth order, see Table 2.1. Thus the reconstruction of this key quantity is the same for CRK4 and CRK5. On the other hand, CRK5 is probably less robust than CRK4 because there are negative constants in the reconstruction of point values and there are negative coefficients in the tableau of the Runge-Kutta scheme.

In the following, we will concentrate on simple Riemann problems, in order to investigate the effectiveness of our schemes to prevent the onset of spurious oscillations.

Next, we consider a Riemann problem due to Lax [12]. Here the initial condition is  $u = u_L$  for  $x \leq 0.5$ , and  $u = u_R$  for  $x > 0.5$ . The computational domain is  $[0, 1]$ , with free-flow boundary conditions. The left (L) and right (R) states are given by:

$$u_L = \begin{pmatrix} 0.445 \\ 0.311 \\ 8.928 \end{pmatrix} \quad u_R = \begin{pmatrix} 0.5 \\ 0. \\ 1.4275 \end{pmatrix}.$$

The inverse of the maximum eigenvalue for this flow is approximately  $c = 0.21$ . As mesh ratio, we thus pick  $\lambda = 0.2\lambda_0$ , where  $\lambda_0$  is, as usual, the mesh ratio obtained with linear stability analysis, see (2.15). This means that the Courant number is very close to the critical one.

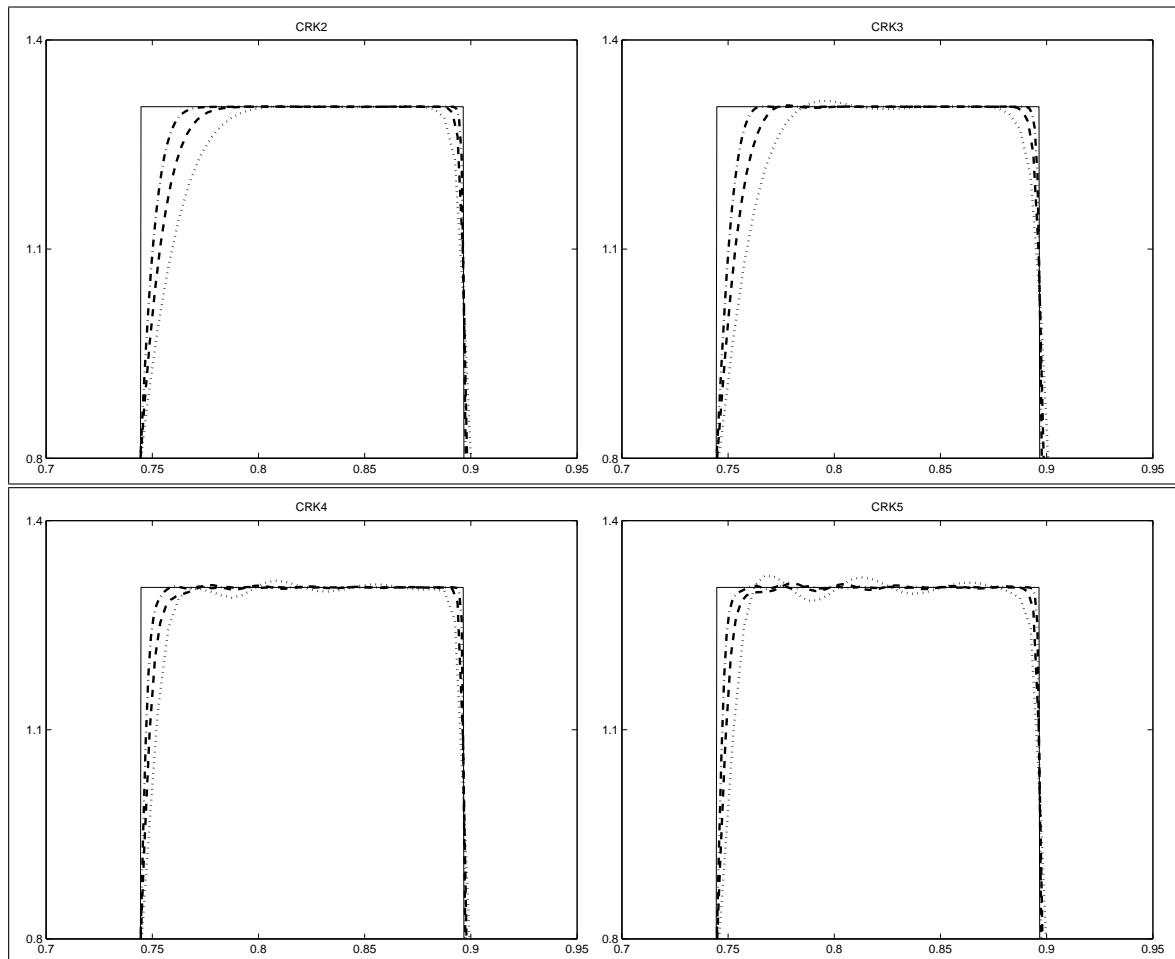


Figure 4.2: Lax' Riemann problem  $\lambda = 0.2\lambda_0$ . Solution given by CRK2, CRK3, CRK4, and CRK5 for  $N = 200$  (dotted line),  $N = 400$  (dashed line) and  $N = 800$  (dash-dotted line).

The results are shown in Fig. 4.2, where a detail in the density peak is shown. The whole solution can be seen for instance in [15] or [26]. The detail we show is a zoom on the region containing spurious oscillations. The discontinuities appearing on the left and on the right of the density peak are respectively a contact and a shock wave. The solution is shown, for all schemes studied here, for  $N = 200$  (dotted line),  $N = 400$  (dashed line) and  $N = 800$  (dash-dotted line). The high order schemes clearly exhibit small amplitude spurious oscillations in this test problem. These oscillations are of ENO type, in the sense that their amplitude decreases as the grid is refined. It can also be noted that the shock is, as expected, better resolved than the contact wave, and the resolution of the contact improves with the order of accuracy.

A 2D application of CRK4 to systems of equations can be found in Fig. 4.3. Here the contour plots of the density for a 2D Riemann problem in gas dynamics are shown. The initial data are derived from Configuration 5 of [13]. This configuration contains jumps in the density and in the components of the velocity parallel to the initial steps in the density. The result is the interaction of four contact waves. Thus, this test is particularly hard for central schemes, which tend to smear contact discontinuities more than upwind schemes.

In this test, the 2D CRK4 scheme is applied componentwise. As in the 1D case, small spurious

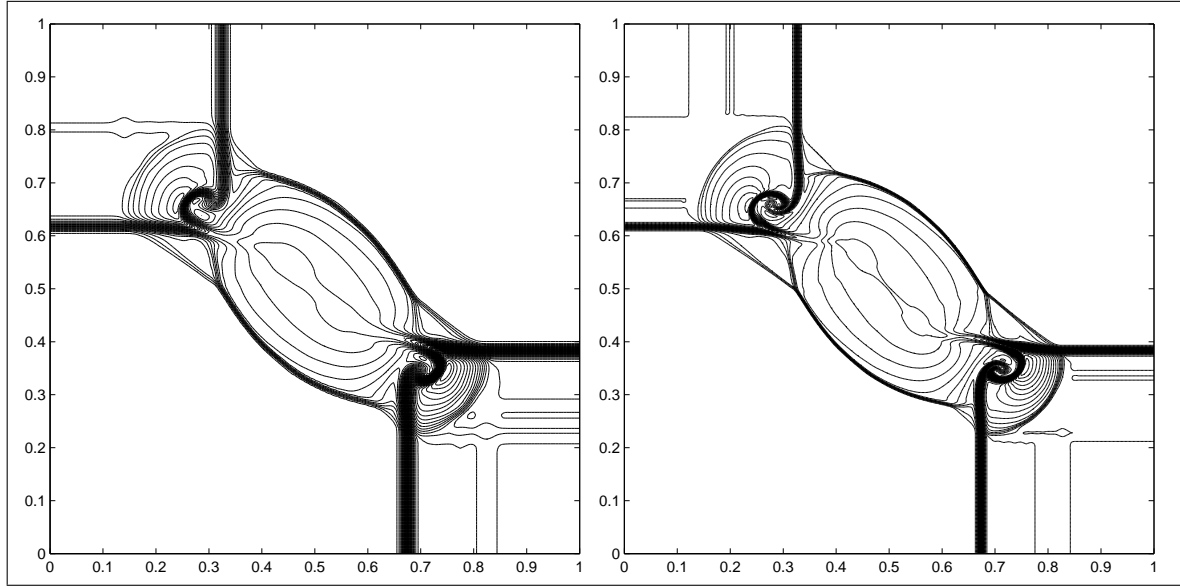


Figure 4.3: Two-dimensional Riemann problem, density. Componentwise application of the 2D CRK4 scheme. Left: 200 by 200 grid; right: 400 by 400 grid,  $T = 0.2$ , 50 level lines

wiggles develop in the states where the solution is uniform. Again, these oscillations are of ENO type: their amplitude decreases under grid refinement. The figure clearly shows the effect of a high order scheme: resolution improves dramatically when the grid is refined from a 200 by 200 to a 400 by 400 mesh, and very fine details become visible.

## 4.2 Projection along characteristic directions

While the results shown in Fig. 4.1 are quite satisfactory, the numerical solutions shown at the bottom of Fig. 4.2 can be improved. The componentwise application of CRK schemes seems to be inadequate whenever discontinuities are separated by regions of almost constant states. It was shown in [26], although in a different context, that spurious wiggles disappear if the Smoothness Indicators are computed after projecting the solution along characteristic directions. Moreover this costly algorithm seems to be needed only once, at the beginning of each time step.

We apply this idea to our 4th and 5th order schemes. Before discussing our numerical results, let us describe the algorithm we consider. We recall that we are supposing that the Jacobian matrix  $A(u)$  of the flux function  $f(u)$  has a complete set of right eigenvectors. Let  $R(u)$  be the non-singular matrix whose columns are the right eigenvectors of  $A(u)$ .

At each grid point  $j$ , compute  $R(\bar{u}_j^n)$ . Let  $\{\bar{u}_{j+l}^n\}$  be the data in the stencil of the  $j$ th cell. For CRK4 and CRK5, the stencil of the reconstruction consists of 5 points; thus  $l = -2, \dots, 2$ . Map each cell average in the stencil of the  $j$ th cell along the characteristic directions, i.e. compute the vectors:

$$\bar{v}_{j+l} = R^{-1}(\bar{u}_j^n) \bar{u}_{j+l}^n \quad l = -2, \dots, 2.$$

Construct a conservative interpolant  $\Pi_v^j$  for the data  $\{\bar{v}_{j+l}\}$  in the sense that:

$$\frac{1}{h} \int_{x_{j+l}-\frac{h}{2}}^{x_{j+l}+\frac{h}{2}} \Pi_v^j(x - x_j) = \bar{v}_{j+l} \quad l = -1, 0, 1.$$

Use the CWENO recipe *componentwise* to compute the non linear weights entering the construction of  $\Pi_v^j$ . Then define the interpolant for the conserved variables  $u$  through the equation:

$$\Pi_u^j(x - x_j) = R(\bar{u}_j^n) \Pi_v^j(x - x_j).$$

Finally, use this function to evaluate the two staggered half-cell averages:

$$\bar{u}_{j,-}^n = \frac{1}{h} \int_{x_j - \frac{h}{2}}^{x_j} \Pi_u^j(x - x_j) dx \quad \bar{u}_{j,+}^n = \frac{1}{h} \int_{x_j}^{x_j + \frac{h}{2}} \Pi_u^j(x - x_j) dx,$$

with  $\bar{u}_{j+1/2}^n = \bar{u}_{j,+}^n + \bar{u}_{j+1,-}^n$  and the point value  $u(x_j, t^n) = \Pi_u^j(0)$ .

**Remark:** The algorithm just described is clearly conservative. In fact:

$$\frac{1}{h} \int_{x_{j+l} - \frac{h}{2}}^{x_{j+l} + \frac{h}{2}} \Pi_u^j(x - x_j) = \frac{1}{h} R(\bar{u}_j^n) \int_{x_{j+l} - \frac{h}{2}}^{x_{j+l} + \frac{h}{2}} \Pi_v^j(x - x_j) = R(\bar{u}_j^n) \bar{v}_{j+l} = \bar{u}_{j+l}^n \quad l = -1, 0, 1.$$

For gas dynamics, see for instance [34], the matrices  $R$  and  $R^{-1}$  are given by:

$$R(u) = \begin{pmatrix} 1 & 1 & 1 \\ v - c & v & v + c \\ H - vc & H - \frac{c^2}{\gamma - 1} & H + vc \end{pmatrix} \quad R^{-1}(u) = \frac{1}{2} \begin{pmatrix} \frac{v}{c} + 1 - Y & -vX - \frac{1}{c} & X \\ 2Y & 2vX & -2X \\ 1 - \frac{v}{c} - Y & -vX + \frac{1}{c} & X \end{pmatrix}, \quad (4.2)$$

where  $v$  is the velocity,  $H = (E + p)/\rho$  is the enthalpy per unit volume,  $c = \sqrt{\gamma p/\rho}$  is the sound speed and  $X = (\gamma - 1)/c^2$ ,  $Y = (H - v^2)X$ .

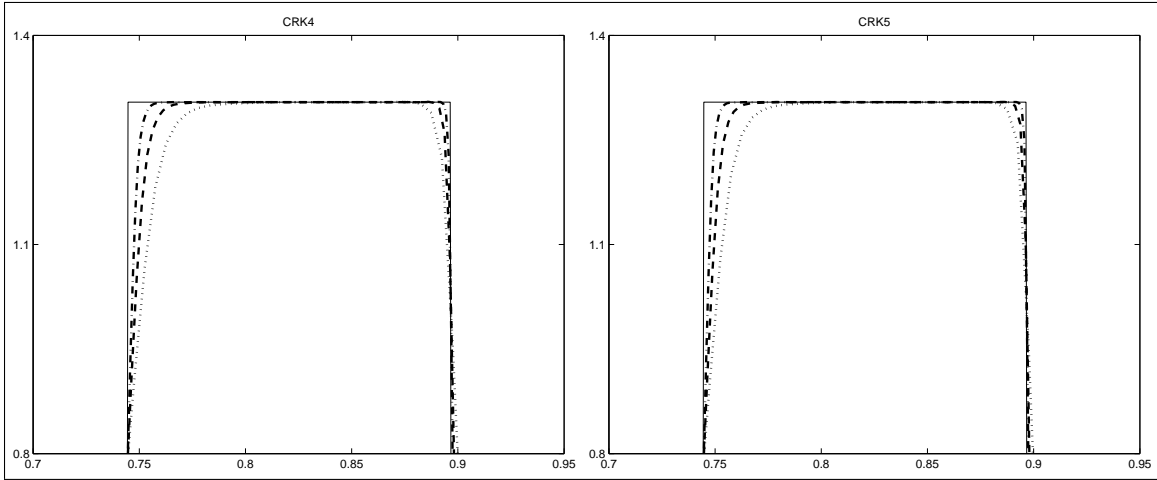


Figure 4.4: Lax' Riemann problem  $\lambda = 0.2\lambda_0$ . Solution given by CRK4 (left) and CRK5 (right) for  $N = 200$  (dotted line),  $N = 400$  (dashed line) and  $N = 800$  (dash-dotted line). The interpolation is computed with projection along characteristic directions.

The results in Fig. 4.4 are obtained using characteristic projection for the evaluation of  $\bar{u}_{j+1/2}^n$  and for the point values  $u(x_j, t^n)$  at time  $t^n$ . Again, this is a detail of the solution to Lax' Riemann problem. The interpolation for the evaluation of the flux derivatives is computed as before componentwise, using the Global Smoothness Indicators, computed once, at the beginning of the time step. Note that the spurious oscillations observed in Fig. 4.2 have disappeared. These results show that even in the context of CRK schemes, projection along characteristics improves the numerical solution. Moreover, it is enough to perform this procedure only once per time step.

The scheme utilizing projection along characteristic directions is more robust than the componentwise algorithm. In fact it is possible to simplify the construction of the flux derivatives, using *linear* weights. That is, the weights  $w_j^k$  in the reconstruction of flux derivatives are simply set to  $w_j^k = C^k$ , where  $C^k$  are the appropriate accuracy constants. We call this strategy *semilinear weights*, because the scheme is non-linear only at the first reconstruction in each time step. The results can be seen in

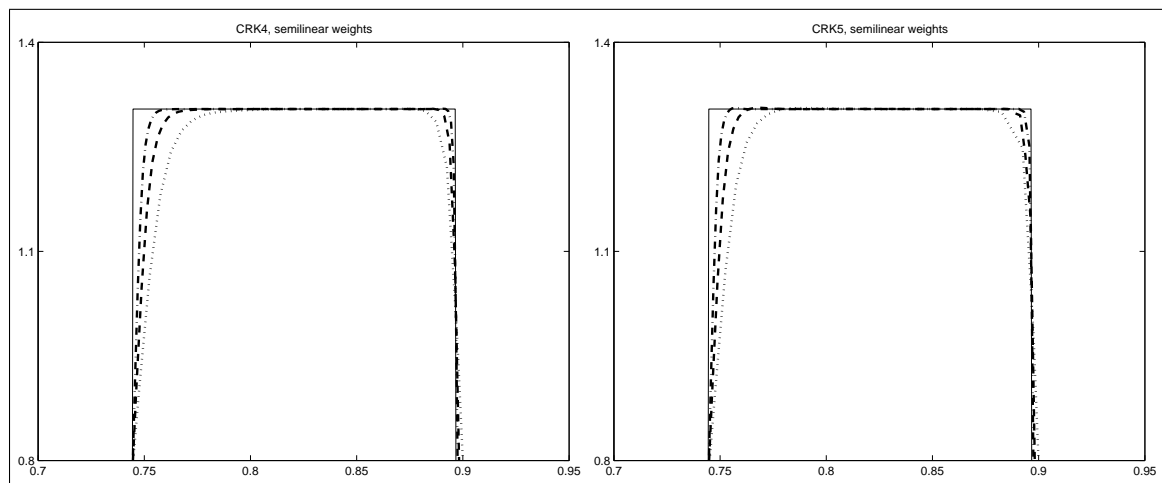


Figure 4.5: Lax' Riemann problem  $\lambda = 0.2\lambda_0$ . Solution given by CRK4 (left) and CRK5 (right) for  $N = 200$  (dotted line),  $N = 400$  (dashed line) and  $N = 800$  (dash-dotted line). The interpolation is computed with projection along characteristic directions, while  $f_x$  is computed with linear weights.

Fig. 4.5. We note that the numerical solution is qualitatively very similar to the one obtained with non linear weights on the fluxes, Fig. 4.4.

A more demanding one dimensional test is the classic Woodward and Colella bang, [36]. Here, the initial data is given by three constant states, namely  $u = u_L$  for  $x \leq 0.1$ ,  $u = u_C$  for  $0.1 < x \leq 0.9$  and  $u = u_R$  for  $x > 0.9$ . The different states are given by:

$$\begin{pmatrix} \rho \\ v \\ p \end{pmatrix}_L = \begin{pmatrix} 1 \\ 0 \\ 1,000 \end{pmatrix} \quad \begin{pmatrix} \rho \\ v \\ p \end{pmatrix}_C = \begin{pmatrix} 1 \\ 0 \\ 0.01 \end{pmatrix} \quad \begin{pmatrix} \rho \\ v \\ p \end{pmatrix}_R = \begin{pmatrix} 1 \\ 0 \\ 100 \end{pmatrix}.$$

The computational domain is  $[0, 1]$  with reflective boundary conditions. The time step was chosen adaptively, namely:

$$\Delta t = 0.9\lambda_0 \frac{h}{\max(|v| + c)},$$

with  $\lambda_0$  given in (2.15). This test provides a complex wave pattern: two strong shocks run against each other, and they eventually collide at  $t \simeq 0.27$ . In the mean time, two strong rarefaction waves bounce against the reflective walls. The reflected waves interact with the shocks, progressively eroding their strength. The solution is shown at  $T = 0.038$ .

In this test, negative undershoots in the pressure and the density may appear as the waves interact. The undershoot is immediately eliminated, when the waves separate. This phenomenon is due to the fact that for one or two time steps, where two discontinuities interact, it is not possible to pick a smooth stencil. Thus, in these instants, the pressure or the density may become negative, and it is not possible to compute the sound speed  $c$ , which is required in the evaluation of  $\Delta t$  and in the computation of the rotation matrices appearing in the projection along characteristics. For these reasons, we defined the sound speed as  $c = \sqrt{\max(0, \gamma p / \rho)}$ . This artifact is not needed in the case of the componentwise implementation.

The results obtained with the CRK4 scheme are shown in Fig. 4.6. The solid line and the dashed line represent the solution obtained with the componentwise algorithm, and with projection along characteristic directions, respectively. It is clear that the componentwise algorithm is more oscillatory, but less diffusive than the algorithm based on projection along characteristic directions.

The scheme based on projection along characteristic directions can be made much more efficient, if projection along characteristic directions is applied selectively, only in those cells close to discontinuities, see [24].

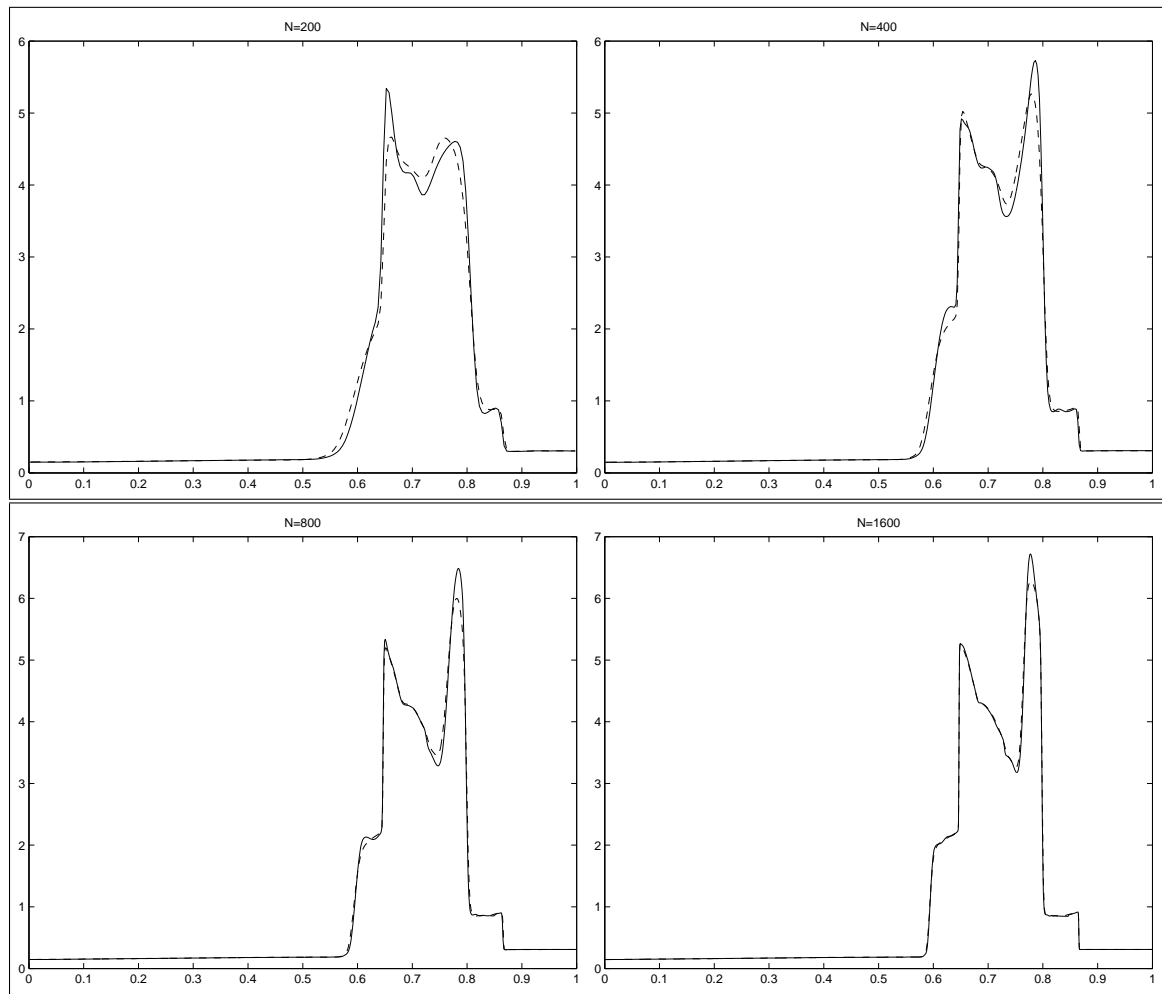


Figure 4.6: Woodward and Colella problem at  $T = 0.038$ . Solution given by CRK4 with (dashed line) and without (solid line) projection along characteristic directions, for several values of  $N$ .

We expect that projection along characteristic directions would cure also the spurious oscillations of the two-dimensional scheme, observed in Fig. 4.3.

## Conclusions

A new class of finite volume central schemes for the numerical approximation of systems of conservation laws is presented. The novelty of the method consists in a new Runge-Kutta type time discretization.

The new method is more efficient than previously developed central WENO schemes, and easier to implement. Several one and two-dimensional numerical tests show the effectiveness of the method.

In particular, the effect of characteristic reconstruction is considered in detail. It is shown that if characteristic variables are used in the CWENO reconstruction needed for the computation of the staggered cell average, then spurious oscillations near discontinuities disappear, while the choice of variables in the reconstruction of pointwise values of the function and of space derivatives of the flux does not seem to have relevant influence on the spurious oscillations. This remarkable phenomenon is still without theoretical explanation, and it is certainly worth further attention.

Characteristic reconstruction is expensive, and it gives better results only near discontinuities, or where the function is less regular. This suggests the use of characteristic variables only where needed,

resulting in an adaptive scheme, which would be virtually oscillation-free, and quite efficient. The construction of such a scheme and its numerical properties are presented in the paper [24]. A more thorough investigation of the advantages of coupling adaptively central schemes with more sophisticated, but slower schemes is being carried out. Several extensions of the present scheme are in order. In particular, we are investigating a finite difference version of the scheme, in which the basic unknowns are approximations of the pointwise values of the field variables. A finite difference approach is desirable for several reasons. First it should provide more efficient high order schemes in several dimensions, as is the case of standard high order finite difference WENO schemes [30]. A second and probably more important reason is that the finite difference approach is more efficient than the finite volume approach for constructing high order schemes for hyperbolic systems with stiff source terms. For these systems, in fact, the source should be treated implicitly, while the hyperbolic term should be treated in an explicit form (because of the nonlinearity of the hyperbolic part, and the consequent nonlinearity of the reconstruction procedure, and the absence of stiffness in the hyperbolic term). The resulting scheme has the form of an IMEX (Implicit-Explicit) time discretization [3], [22]. This approach is presently under investigation.

## Acknowledgments

The authors would like to thank Referee n.2 for carefully reading the paper and pointing out several small mistakes.

## References

- [1] Arminjon P., Stanescu D., Viallon M.-C., *A Two-Dimensional Finite Volume Extension of the Lax-Friedrichs and Nessyahu-Tadmor Schemes for Compressible Flow*, Proc. 6th. Int. Symp. on CFD, Lake Tahoe, 1995, M. Hafez and K. Oshima, editors, Vol. IV, pp.7–14.
- [2] Arminjon P., Viallon M.C., Madrane A., *A finite volume extension of the Lax-Friedrichs and Nessyahu-Tadmor schemes for conservation laws on unstructured grids*, Int. J. Comp. Fluid Dyn., 9 (1997), 1–22.
- [3] Asher U., Ruuth S., and Spiteri R.J., *Implicit-explicit Runge-Kutta methods for time dependent Partial Differential Equations*, Appl. Numer. Math. 25, (1997), 151–167.
- [4] Bianco F., Puppo G., Russo G., *High Order Central Schemes for Hyperbolic Systems of Conservation Laws*, SIAM J. Sci. Comp., 21 (1999) no 1, 294–322.
- [5] A. Harten and S. Osher, *Uniformly high-order accurate nonoscillatory schemes. I.*, SIAM J. Numer. Anal., **24** (2) 279 (1987).
- [6] Hu C., Shu C.-W., *Weighted Essentially Non-Oscillatory Schemes on Triangular Meshes*, ICASE report N<sup>o</sup> 98-32 (submitted to JCP).
- [7] Jiang G.-S., Shu C.-W., *Efficient Implementation of Weighted ENO Schemes*, J. Comput. Phys., **126**, (1996), 202–228.
- [8] Jiang G.S., Tadmor E., *Nonoscillatory central schemes for multidimensional hyperbolic conservation laws*, SIAM J. Sci. Comp., 19 (1998), 1892–1917.
- [9] Jin S., Xin Z., *The Relaxation Schemes for Systems of Conservation Laws in Arbitrary Space Dimensions*, Comm. Pure Appl. Math., **48**, (1995), 235–276.
- [10] Kurganov A., Tadmor E., *New high-resolution central schemes for nonlinear conservation laws and convection-diffusion equations*, J. Comput. Phys. **160** (2000), no. 1, 241–282.
- [11] Lambert J.D., *Numerical Methods for Ordinary Differential Systems. The Initial Value Problem*, John Wiley & Sons, Chichester, 1991.

- [12] Lax P.D., *Weak Solutions of Non-Linear Hyperbolic Equations and Their Numerical Computation*, CPAM **7** (1954), 159-193.
- [13] Lax, P.D., Liu X.D., *Solution of Two-Dimensional Riemann Problems of Gas-Dynamics by Positive Schemes*, SIAM J. Sci. Comp. **19**, no. 2 (1998), 319-340.
- [14] LeVeque R.J., *Finite Volume Methods for Hyperbolic Problems*, Cambridge Texts in Applied Mathematics, Cambridge University Press, Cambridge, UK (2002).
- [15] Levy D., Puppo G., Russo G., *Central WENO Schemes for Hyperbolic Systems of Conservation Laws*, Math. Model. and Numer. Anal., **33**, no. 3 (1999), 547–571.
- [16] Levy D., Puppo G., Russo G., *Compact Central WENO Schemes for Multidimensional Conservation Laws*, SIAM J. Sci. Comp., **22**, (2000), 656–672.
- [17] Levy D., Puppo G., Russo G., *A fourth order central WENO scheme for multi-dimensional hyperbolic systems of conservation laws*, to appear on SIAM J. Sci. Comp.
- [18] Lin C.T., Tadmor E., *High resolution nonoscillatory central schemes for Hamilton-Jacobi equations*, SIAM J. Sci. Comp., 21 (2000), 2163–2186.
- [19] Liotta S. F., Romano V., Russo G., *Central schemes for balance laws of relaxation type*, SIAM J. Numer. Anal., **38**, (2000), 1337–1356.
- [20] Nessyahu H., Tadmor E., *Non-oscillatory Central Differencing for Hyperbolic Conservation Laws*, J. Comput. Phys., **87**, no. 2 (1990), 408–463.
- [21] Pareschi L., *Central differencing based numerical schemes for hyperbolic conservation laws with relaxation terms*, SIAM J. Numer. Anal. 39 (2001), no. 4, 1395–1417.
- [22] Pareschi L., Russo G., *Implicit-Explicit Runge-Kutta schemes for stiff systems of differential equations*, Recent Trends in Numerical Analysis, Edited by L.Brugnano and D.Trigiantè, Advances in Computation, Vol. 3 (2000), 269–289.
- [23] Puppo G., *Numerical entropy production for central schemes*, submitted to SIAM J. Sci. Comp.
- [24] Puppo G., *Adaptive application of characteristic projection for central schemes*, to appear on the proceedings of the HYP2002 conference.
- [25] Romano V., Russo G., *Numerical solution for hydrodynamical models of semiconductors*, Math. Models Methods Appl. Sci., 10 (2000), 1099–1120.
- [26] Qiu J, and Shu C.W., *On the construction, comparison, and local characteristic decomposition for high order central WENO schemes*, submitted to J. Comput. Phys.
- [27] Russo G., *Central Schemes and Systems of Balance Laws*, in “Hyperbolic Partial Differential Equations, Theory, Numerics and Applications”, edited by Andreas Meister and Jens Struckmeier, Vieweg, Göttingen, 2002.
- [28] Sanders R., Weiser A., *A High Resolution Staggered Mesh Approach for Nonlinear Hyperbolic Systems of Conservation Laws*, JCP, **1010**, (1992), 314–329.
- [29] Shi J., Hu C., Shu C.W., *A technique of treating negative weights in WENO schemes*, submitted to JCP.
- [30] Shu C.-W., *Essentially Non-Oscillatory and Weighted Essentially Non-Oscillatory Schemes for Hyperbolic Conservation Laws* in Advanced Numerical Approximation of Nonlinear Hyperbolic Equations, Lecture Notes in Mathematics (editor: A. Quarteroni), Springer, Berlin, 1998.
- [31] Shu, C.W., *Numerical Experiments on the accuracy of ENO and modified ENO schemes*, J. Sci. Comp., **5**, vol. 2, (1990), 127–149.

- [32] Shu C.-W., Osher S., *Efficient Implementation of Essentially Non-oscillatory Shock-Capturing Schemes, II*, J. Comput. Phys., **83**, 1989, 32–78.
- [33] Spiteri R.J., Ruuth S.J., *A New Class of Optimal High-Order Strong-Stability-Preserving Time Discretization Methods*, SIAM J. Numer. Anal. **40** (2002), no. 2, 469–491.
- [34] Stiriba Y., Marquina A., Donat R., *Equilibrium real Gas Computations using Marquina’s scheme*, preprint, 2000.
- [35] Tadmor E., *Approximate Solutions of Nonlinear Conservation Laws*, in Advanced Numerical Approximation of Nonlinear Hyperbolic Equations, Lecture Notes in Mathematics (editor: A. Quarteroni), Springer, Berlin, 1998.
- [36] Woodward P., Colella P., *The Numerical Simulation of Two-Dimensional Fluid Flow with Strong Shocks*, J. Comput. Phys., **54**, 1984, 115–173.
- [37] Zennaro M., *Natural Continuous Extensions of Runge-Kutta Methods*, Math. Comp., **46**, (1986), 119–133.